RSC Advances

PAPER

View Article Online
View Journal | View Issue

Cite this: *RSC Adv.*, 2019, **9**, 2892

Bi-functional titanium-polydopamine-zinc coatings for infection inhibition and enhanced osseointegration

Lei Wang,†[a] Xifu Shang,†[b] Yuefeng Hao,†[c] Guoyang Wan,[c] Lijun Dong,[a] Degang Huang,[a] Xin Yang,[a] Junying Sun,[d] Qiang Wang,*[a] Guochun Zha*[e] and Xing Yang*[c]

The ideal orthopedic implant coating is expected to both inhibit microbial infection and promote osseointegration. In this study, Zn ions were immobilized on a Ti substrate *via* a polydopamine (PDA) chemical surface modification to prepare Ti-PDA-Zn coatings. Scanning electron microscopy (SEM), atomic force microscopy (AFM), energy-dispersive X-ray spectroscope (EDS), X-ray photoelectron spectroscopy (XPS), contact analysis system, and inductively coupled plasma atomic emission spectrometry (ICP-AES) were used to analyze the morphology, composition, wettability, and zinc ions release of the coatings. The Ti-PDA-Zn coatings demonstrated excellent antibacterial activities *in vitro* against both *Staphylococcus aureus* and *Escherichia coli*. The coatings additionally displayed good biocompatibility, as confirmed by cytoskeletal observations and cell viability assays. Furthermore, the *in vivo* results confirmed the excellent antibacterial properties and improved osseointegration capability of the Ti-PDA-Zn coating in the presence of *S. aureus*. The present findings indicate that the Ti-PDA-Zn coatings prepared herein have potential application in orthopedic implantation.

Received 3rd November 2018
Accepted 9th January 2019

DOI: 10.1039/c8ra09112a

rsc.li/rsc-advances

Introduction

Titanium and its alloys have been used widely to fabricate dental and orthopedic implants because of their low elastic modulus, good mechanical strength, and excellent cytocompatibility.[1] Despite great promise in clinical practice, the effective application of device implants is hindered by the occurrence of implant-associated infections (IAIs) after device implantation.[2,3] For example, the annual infection rate for indwelling orthopedic devices is 4.3% in the USA.[4] The infection rate of joint replacements is approximately 1%. In the case of revision surgeries, the infection rate is higher.[5] Upon the onset of IAIs, bacteria tend to aggregate in a hydrated polymeric matrix to form a biofilm on the implant surface and are difficult to eradicate as they are resistant to antibiotics, immune cells, and other potential infection defense mechanisms.[6] In addition, such infection and inflammation reactions can compromise bone integration and cause implant loosening.[7,8] As a result, complex revision surgeries and prolonged hospitalization, with generally high associated medical costs, are often inevitable.[9,10] Therefore, the engineering of implant surfaces with reduced infection risks and improved osseointegration capabilities is highly desirable for the clinical success of established titanium implants (Scheme 1).

Recently, zinc has attracted growing attention for various biomedical applications owing to its excellent antibacterial properties and biological activity. It has been proven that zinc ions can interfere with multiple bacteria-related activities, including transmembrane proton translocation, glycolysis, and acid tolerance.[11] Hu *et al.* have reported that Zn-implanted TiO_2 coatings exhibited good antibacterial effects against both *Escherichia coli* (*E. coli*) and *Staphylococcus aureus* (*S. aureus*) as well as excellent biocompatibility.[12] Wang *et al.* reported the fabrication of ZnO-modified titanium surfaces that not only exhibited broad-spectrum antibacterial properties, but also could suppress the formation of a bacterial biofilm.[13] Furthermore, extensive research has confirmed the excellent biological activity of zinc. For instance, Liang *et al.* demonstrated that Zn-modified Ti substrates could improve osteoblast biocompatibility by inhibiting MG-63 apoptosis and otherwise promoting its proliferation.[14] Yusa *et al.* developed a zinc-modified titanium surface that could up-regulate expression of osteoblast-related genes.[15] Shen *et al.* demonstrated that Zn-incorporated

[a]*Department of Orthopedics, The First Affiliated Hospital of Wannan Medical College, Wuhu 241001, Anhui, China. E-mail: 13909636163@126.com*

[b]*Department of Orthopedics, The First Affiliated Hospital, University of Science and Technology of China, Hefei 230001, Anhui, China*

[c]*Department of Orthopedics, Affiliated Suzhou Hospital of Nanjing Medical University, Suzhou 215500, Jiangsu, China. E-mail: xingyangsz@126.com*

[d]*Department of Orthopedics, The First Affiliated Hospital of Soochow University, Suzhou 215000, Jiangsu, China*

[e]*Department of Orthopedic Surgery, Affiliated Hospital of Xuzhou Medical University, Xuzhou 221002, Jiangsu, China. E-mail: 41049015@qq.com*

† These authors contributed equally to this study.

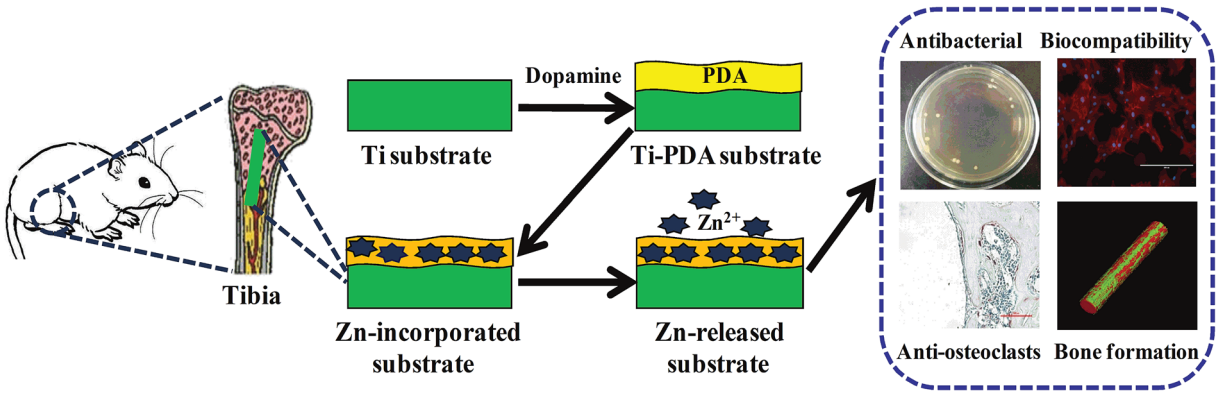

Scheme 1 Schematic diagram of the study.

microrough titanium coatings could enhance bone formation by regulating the proliferation or differentiation of both osteoblasts and osteoclasts.[16] These studies show that the incorporation of zinc into implants is an ideal approach to endow the implants with both antimicrobial and osteogenic activities.

To date, several methodologies to incorporate zinc into various types of biomaterials have been reported, including plasma spraying,[17] magnetron sputtering,[18] plasma immersion ion,[19] plasma electrolytic oxidation,[20] and sol–gel[21] methods. However, most of these approaches require special equipment and sophisticated technologies. Alternatively, inspired by the adhesive proteins, Mfp-5, secreted by mussels in nature, polydopamine (PDA) coatings are generating much interest for use in the surface modification of metallic implants.[22,23] Under weak alkaline conditions, the polymerization of dopamine is achieved by oxidation of the dopamine to dopamine quinone and formation of 5,6-dihydroxyindole through intermolecular cyclization, the material formed can be deposited as a thin polymerized coating layer on diverse types of material surfaces *via* covalent and/or non-covalent bonding.[24] Previous studies have demonstrated the use of polydopamine in successfully depositing active metal ions (*e.g.*, Ag, Cu, Zn) on various materials.[25–27] Moreover, numerous studies have confirmed that polydopamine coatings can improve the hydrophilicity and biocompatibility of a biomaterial.[28–30]

In the present study, polydopamine-functionalized titanium substrates were fabricated and subsequently treated with $ZnCl_2$ solution to achieve dual-functionality on the Ti implants. Animal models were used to test the antimicrobial effect and the osteogenic potential of the Ti-PDA-Zn coatings in the presence of bacteria. *In vitro* studies were performed to assess whether the Ti-PDA-Zn coatings could endow the Ti implants with both good self-antibacterial performance and biocompatibility. In the *in vivo* studies, the Ti-PDA-Zn coatings were implanted in a rat model to examine the antibacterial and osseointegration performance of the coatings. As the relationship between *S. aureus* and osteoclasts is rarely examined,[31] tartrate-resistant acid phosphatase (TRAP) staining and diaminobenzidine (DAB) staining of murine monoclonal antibodies were used to assess the influence of *S. aureus* on osteoclast activity. The findings showed that the Ti-PDA-Zn coatings exhibited both excellent antimicrobial and osseointegration properties. To our knowledge, this is the first study reporting the preparation of zinc-coated PDA-modified titanium surfaces with such dual functionalities.

Materials and methods

Preparation of Ti-PDA

Pure Ti plates with dimensions of 5.8 mm × 5.8 mm × 1 mm and 13 mm × 13 mm × 1 mm (length × width × thickness) were used for the *in vitro* studies. For the *in vivo* experiments, pure Ti rods with dimensions of 10 mm × 1.2 mm (length × diameter) were used. These materials were supplied by Tianjin Zhengtian Medical Device Company (Tianjin, China). Prior to PDA coating, the Ti plates and rods were washed sequentially with acetone, ethanol, and deionized water under ultrasonication. Dopamine solution (2 mg mL^{-1}) was prepared by dissolving dopamine hydrochloride (400 mg; Sigma, MO, USA) in Tris–HCl buffer (200 mL; 10 mM, pH = 8.5). The titanium plates and rods were then soaked in the dopamine solution for 24 h for PDA coating. The PDA-decorated titanium substrates (Ti-PDA) were ultrasonically cleaned using deionized water and dried overnight in a vacuum oven at room temperature.

Fabrication of Ti-PDA-Zn

Zinc ions were immobilized on the PDA coatings *via* soaking. A solution of $ZnCl_2$ (Acros Reagent Co. Ltd., Geel, Belgium) in deionized water was first prepared to achieve a Zn concentration of 0.2 mol L^{-1}. The Ti-PDA substrates were then immersed in the solution for 30 min to anchor Zn ions onto the surfaces; the resulting substrates are referred to as Ti-PDA-Zn. Finally, the coatings were ultrasonically cleaned using deionized water, air-dried, and sterilized by irradiation prior to subsequent experiments.

Characterization

The surface morphologies of the pure Ti, Ti-PDA, and Ti-PDA-Zn substrates were observed using scanning electron microscopy (SEM; S-3400, Hitachi, Tokyo, Japan) and atomic force microscopy (AFM; XE-100, Park Systems, USA). The elemental

composition of the samples was determined by energy-dispersive X-ray spectroscopy (EDS, QX200, Bruker, Germany) and X-ray photoelectron spectroscopy (XPS; PHI 5802, Physical Electronics, London, UK). The Zn, N, C, O, and Ti profiles were acquired by XPS in conjunction with Ar ion bombardment at a sputtering rate of ~4 nm min^{-1}. The surface wettability of the substrates was assessed using a contact analysis system (DSA 25S, Kruss GmbH, Hamburg, Germany); three replicates were measured per sample. All measurements were conducted at room temperature.

Zinc ion release

The Ti-PDA-Zn samples were immersed in phosphate-buffered saline solution (10 mL; PBS; Hyclone, UT, USA) and incubated at 37 °C in the absence of stirring for 1, 4, 7, and 14 days. These time points were selected according to the biocompatibility tests. The amount of zinc ions released at different intervals of time was measured by inductively coupled plasma atomic emission spectrometry (ICP-AES, Leeman, Ohio, USA). Three samples were used per measurement.

Cell culture

MC3T3-E1 mouse preosteoblasts (CRL-2594, subclone 14, ATCC) were used to evaluate the biocompatibility of the samples. The cells were incubated at 37 °C in a 5% CO_2 environment in α-minimum essential medium with 10% fetal bovine serum and 1% streptomycin/penicillin. The cells were subcultured every 3 days, washed twice with PBS and incubated in a 0.5 g L^{-1} trypsin/0.2 g L^{-1} ethylenediaminetetraacetic acid (EDTA) solution (Gibco) for 2 min at 37 °C to detach cells from the base of the culture flasks. The subcultured cell solution was then centrifuged at 1000 rpm for 3 min and resuspended in the complete medium for reseeding on the various surfaces. The cells were seeded at a density of 1×10^4 cells per well in a 96-well plate and 2×10^4 cells per well in a 24-well plate.

Cell morphology observations

The cells were cultured on Ti, Ti-PDA, and Ti-PDA-Zn substrates (5.8 mm in diameter) in 96-well plates. After 1 day of culture, the samples were washed with PBS and then fixed using 2.5% glutaraldehyde (Sigma, St. Louis, MO, USA) in PBS for 1 h and then rinsed three times with PBS for 10 min. Then, the cells were dehydrated in a graded series of ethanol (30%, 50%, 70%, 90%, and 100%) for 30 min each and left in 100% ethanol. The samples were dried using a Critical Point Dryer (CPD030, Leica, Wetzlar, Germany) and sputter-coated gold using an Ion Sputter (SC7620, Quorum Technologies, Lewes, UK) prior to SEM examination. Finally, the morphology of the cells on the surface of the disks was observed by SEM (SEM, S-3400, Hitachi, Tokyo, Japan).

Cytoskeletal observations

After culturing for 1 day, the cells seeded on the test samples (plates of 13 mm × 13 mm × 1 mm) at a density of 2×10^4 cells were briefly rinsed in PBS and fixed for 20 min in 4% paraformaldehyde at room temperature. After three rinses with PBS, the cells were permeabilized for 25 min in 0.2% Triton X-100 (Sigma, Shanghai, China) and blocked in 0.1% bovine serum albumin (Sigma, Shanghai, China) in PBS at room temperature in the dark. The cells were then stained in the dark using rhodamine-phalloidin and 4′,6-diamidino-2-phenylindole. Finally, fluorescence images of the cell morphology and cytoskeletal arrangement were obtained on an EVOS fluorescence microscope (AMG, Thornwood, NY, USA).

Cell viability assays

Cell proliferation was evaluated using cell counting kit-8 assays (CCK-8, Dojindo Laboratories, Tokyo, Japan). Samples with dimensions of 5.8 mm × 5.8 mm × 1 mm were placed in a 96-well plate. The cell concentration was 1×10^4 cells per well. After 1, 4, and 7 days of culture, the cells were washed twice with PBS. The CCK-8 reagent (100 μL) was then added to each well following the manufacturer's directions. After 2 h of incubation under a 5% CO_2 atmosphere, the absorbance of the solution was measured at a wavelength of 450 nm using a spectrophotometric microplate reader (Bio-Rad 680, CA, USA). The relative growth rate (RGR) was calculated to analyze the cytocompatibility of the substrates using the following formula:

$$RGR = (OD_{sample}/OD_{blank}) \times 100\%$$

where OD_{sample} is the optical density of the Ti, Ti-PDA, or Ti-PDA-Zn samples and OD_{blank} is the optical density of the blank control sample (α-minimum essential medium).

Antibacterial testing

Plate-counting schemes and live/dead staining were used to investigate the antimicrobial activity of the samples. Gram-positive *S. aureus* (ATCC 25923) and Gram-negative *E. coli* (ATCC 25922) were selected as the pathogenic microbes. The samples were first sterilized in 75% ethanol for 2 h and rinsed three times with sterile PBS. Subsequently, a suspension containing the bacteria at a concentration of 10^6 cfu mL^{-1} was introduced onto the sample surface to a density of 100 μL cm^{-2}. After incubation at 37 °C for 24 h, the dissociated bacteria were collected and inoculated onto a standard agar culture plate for 24 h. The antibacterial rate was calculated using the following formula: antibacterial rate (%) = (CFU of control − CFU of experimental group)/CFU of control × 100%, where a pristine Ti sample served as the control, and Ti-PDA and Ti-PDA-Zn samples constituted the experimental groups.

The planktonic bacteria cultured on the tested samples were removed and 100 μL of the Live/Dead BacLight staining reagent mixture were added. After staining for 15 min in darkness, the adherent bacteria on the samples were observed with fluorescence microscopy (AMG, Thornwood, NY, USA).

Animal studies

A total of 12 male Sprague Dawley (SD) rats (weighing 300–350 g) were used for the studies. Four SD rats were allocated to each substrate (Ti, Ti-PDA, and Ti-PDA-Zn), correspondingly forming

three groups. The rats were anaesthetized with 4% chloral hydrate (0.9 mL per 100 g) prior to surgery. The metaphysis of left tibiae was chosen as the surgical site. After the operating field was shaved and disinfected with iodine, a longitudinal skin incision was made at the proximal tibial metaphysis of the tibia. When the left proximal tibial was exposed by skin incision, a hole was drilled through the proximal tibial metaphysis with a circular drill (1.2 mm diameter) to access the medullary cavity. Then, a 10^4 cfu mL^{-1} *S. aureus* suspension (20 μL) was injected into the medullary cavity with a microsyringe and the sterile Ti rods were inserted. Finally, the fascia and skin were sutured in a single knot technique (4-0 Prolene, Fa. Ethicon, Norderstedt, Germany). After surgery, the rats were housed in ventilated rooms and given access to water and food. This study was performed in strict accordance with the NIH guidelines for the care and use of laboratory animals (NIH Publication no. 85-23 Rev. 1985) and was approved by the Institutional Animal Care and Use Committee of Nanjing Medical University (Nanjing, China).

Micro-CT evaluation

To evaluate new bone formation around the implants, the specimens were scanned using a high-resolution micro-CT scanner (SkyScan1076, Aartselaar, Belgium) at 65 kV using a 1 mm Al filter with a resolution of 18 μm. The three-dimensional (3D) high-resolution reconstructed images were obtained using the software provided by the manufacturer. A region of interest (ROI) with a radius of 1.4 mm from the rods was selected for analysis.

Histological analysis and immunohistochemistry

After 4 weeks and micro-CT scanning, all animals were euthanized by overdose of chloral hydrate. Four left tibiae in each group were removed and fixed in 4% paraformaldehyde for 48 h. Then, the samples were decalcified using 10% EDTA solution for 28 days. All Ti rods were then carefully removed to avoid damage of the newly formed bone tissue, then dehydrated in graded ethanol and embedded in paraffin. Transverse sections (5 μm thick) were collected and stained with hematoxylin-eosin (H&E). Masson's trichrome staining was used to assess the extent of bacterial infection and osseointegration *in vivo*. The TRAP staining kit (Sigma, St. Louis, MO, USA) was used to assess osteoclast activity. DAB staining of the murine monoclonal antibody (ab37644; Abcam plc, Cambridge, UK) was performed to investigate the presence of *S. aureus*, as previously reported.[32]

Statistical analysis

All data are provided as the mean ± standard deviation (S.D.). The statistical analyses were performed by GraphPad Prism 5. One-way analysis of variance (ANOVA) tests and student *t*-tests were used. A difference between two groups was considered statistically significant if $p < 0.05$.

Results

Material surface characterization

The surface morphologies of the samples were examined by SEM (Fig. 1). Both the Ti substrate and Ti-PDA coating displayed similar surface morphologies. In contrast, the Ti-PDA-Zn coating was rougher, and uniformly formed Zn ion particles could be observed on the surface of the coating. These morphological differences were also confirmed by AFM (Fig. 2). The root-mean-square roughness was significantly increased from 16.31 nm for the pristine Ti to 55.01 nm after PDA treatment. After further decoration with Zn, the roughness changed slightly to 53.59 nm. The EDS results further confirmed the successful deposition of Zn ions on the surface of Ti-PDA-Zn, as indicated by the presence of elemental Zn compared with the Ti and Ti-PDA samples (Fig. 3). In addition, XPS survey spectra of the Ti, Ti-PDA, and Ti-PDA-Zn films were collected as shown in Fig. 4. Ti and O peaks could be detected in all samples. In addition, N peaks at 399.9 eV and Zn peaks at 1021.7 eV were observed in the Ti-PDA-Zn films, indicating the successful preparation of the PDA coating and immobilization of the Zn ions. The content of Zn was calculated to be ~6.26%. A C signal was also observed in all the samples, mainly attributed to surface contamination. The surface wettability of the films was determined and the results are shown in Fig. 5. The water contact angles on Ti-PDA and Ti-PDA-Zn were 15.8 ± 1.9 and 18.7 ± 2.1°, respectively, which were significantly lower than that on pure Ti (57.1 ± 3.2°), suggesting that the PDA coating greatly improved the surface wettability of the titanium.

Zinc ion release

To investigate the influence of the biological environment on the Ti-PDA-Zn coating, the amount of released Zn ions was measured by ICP-AES (Fig. 6). In the first 24 h of testing, the Ti-PDA-Zn sample released 0.71 ± 0.07 ppm of Zn ions, and within one week, approximately 1.67 ± 0.04 ppm of zinc ions were released from the Ti-PDA-Zn sample. The relatively fast Zn ion release observed in the first week of testing subsequently gradually decreased, and the total amount of Zn ions released reached 1.70 ± 0.07 ppm by the end of the immersion test.

Cell morphology and cytoskeletal structures

Fig. 7 shows the morphology of MC3T3-E1 cells cultured on different samples. There seems to be little difference in cell morphology. However, the cell numbers on the surfaces of the Ti-PDA and Ti-PDA-Zn samples were significantly higher than on the surface of Ti, which might be attributed to the enhanced biocompatibility of the PDA coating. The cytoskeletal structure of the MC3T3-E1 cells was observed by fluorescence microscopy (Fig. 8). Compared with the cells cultured in the presence of Ti-PDA and Ti-PDA-Zn, the cells cultured in the presence of pure Ti were spread relatively poorly with a spindle shape, and seemed to lack microfilaments. Furthermore, MC3T3-E1 cells cultured at a higher density on the surfaces of Ti-PDA and Ti-PDA-Zn films exhibited better cell spreading, as indicated by the irregular morphology with the development of numerous

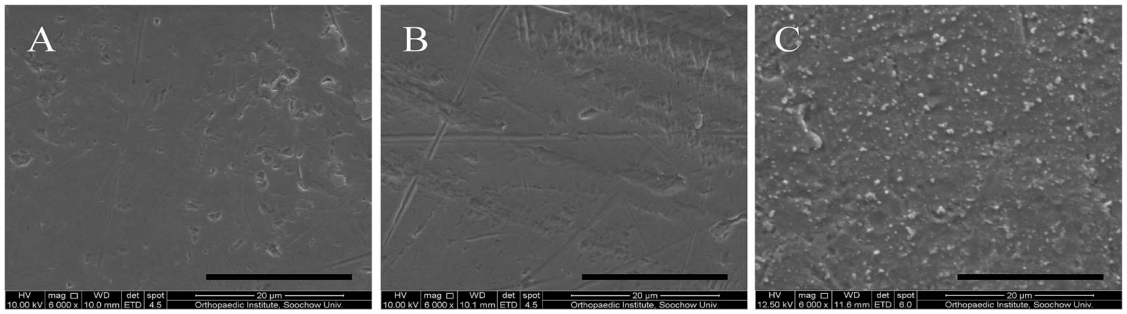

Fig. 1 SEM images of Ti (A); Ti-PDA (B); Ti-PDA-Zn (C). Scale bars, 20 μm.

lamellipodia and filopodia processes. These results indicated that a PDA coating can promote cellular initial adhesion and spreading.

Cell viability assays

The effect of the different samples on the proliferative activity of MC3T3-E1 cells was examined by CCK-8 assay. Fig. 9A shows the OD values measured after 1, 4, and 7 days of incubation. After 1 and 4 days of incubation, no differences in the OD values could be observed for all three samples. However, cell proliferation on the Ti sample was superior to that on the Ti-PDA and Ti-PDA-Zn samples ($p < 0.05$) after 7 days of incubation. In addition, no differences could be found in the OD values between the Ti-PDA and Ti-PDA-Zn samples. Fig. 9B shows the calculated RGRs of the MC3T3-E1 cells on the different samples and for different cultivation periods. According to the standard, a biomaterial with a cytotoxicity of grade 0 or grade 1 when RGR is 90–100% or 75–90%, respectively, implies that this material exhibits no toxicity to the cell. As observed in our studies, the RGR values obtained for the different samples at the different culture times examined were all greater than 75%, indicating that Ti, as well as Ti-PDA and Ti-PDA-Zn showed no cytotoxicity to the MC3T3-E1 cells. Thus, Ti-PDA and Ti-PDA-Zn possess good cell biocompatibility similar to Ti.

Antibacterial testing

Fig. 10 shows representative images of bacteria colonies on Ti, Ti-PDA, and Ti-PDA-Zn after 24 h of incubation. Numerous bacterial colonies were found on the Ti and Ti-PDA samples, suggesting that both samples did not have any antibacterial properties. In contrast, only several colonies were observed on the Ti-PDA-Zn sample, which demonstrated that Ti-PDA-Zn exhibited a very high antibacterial ability. After exposure to the fluorescent stain, live bacteria with intact membranes appear green while dead bacteria with damaged membranes appear red. As shown in Fig. 11, the vast majority of bacteria on Ti and Ti-PDA were viable, but the majority of bacteria on Ti-PDA-Zn were inactivated. The calculated antibacterial rates for Ti-PDA and Ti-PDA-Zn against *S. aureus* and *E. coli* using the plate-counting method are shown in Fig. 12. The antibacterial rates against *S. aureus* for Ti-PDA and Ti-PDA-Zn were 20.5% and 94.1%, respectively. For *E. coli*, the same trend was obtained; the antibacterial rates for Ti-PDA and Ti-PDA-Zn were 17.9% and 89.5%, respectively.

Micro-CT evaluation

Micro-CT was used to analyze the formation and integration of new bone after implantation for 4 weeks; representative micro-CT images are depicted in Fig. 13A–C. The Ti and Ti-PDA implants were surrounded by only a few bone trabeculae. In comparison, more bone trabeculae could be observed around the Ti-PDA-Zn implant. These results were confirmed by the BV/TV data (Fig. 13D). Under the same threshold and volume of interest (VOI) for CT scanning, the Ti-PDA-Zn implant exhibited a higher percentage of BV/TV than the Ti and Ti-PDA implants, indicating that the Ti-PDA-Zn sample possessed enhanced osseointegration performance.

Histological analysis and immunohistochemistry

The transverse decalcified sections of the rat tibia from the different groups examined are shown in Fig. 14 and 15. H&E and Masson's trichrome staining were used to observe

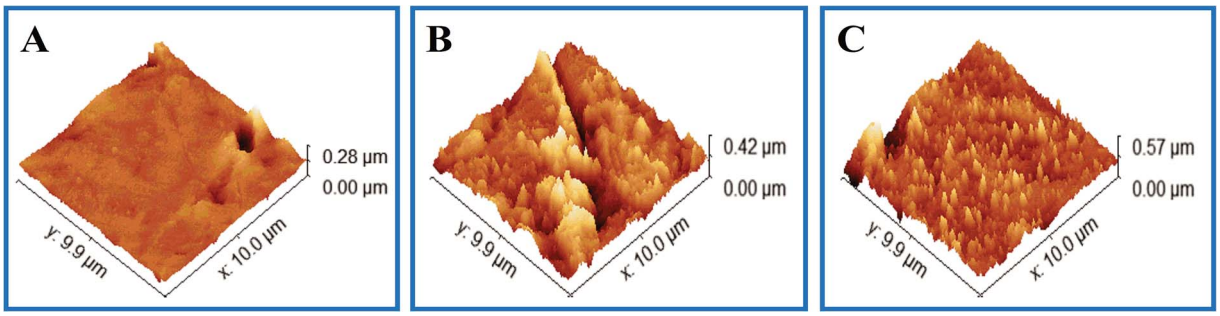

Fig. 2 3D topographical AFM images of Ti (A); Ti-PDA (B); Ti-PDA-Zn (C).

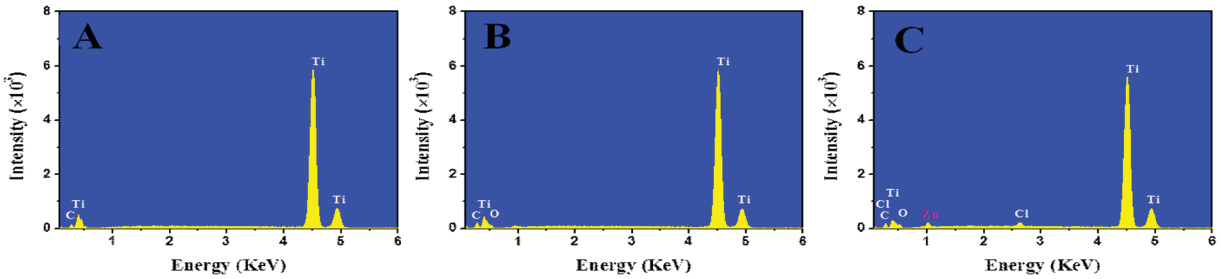

Fig. 3 EDS spectrum of Ti (A); Ti-PDA (B); Ti-PDA-Zn (C).

bacterial infection and osseointegration, while osteoclast activity and bacterial residue were confirmed by TRAP staining and immunohistochemical analysis. Four weeks after surgery, the bone tissues around the Ti and Ti-PDA implants were destroyed by bacterial infection, as confirmed by the large number of neutrophils observed inside the medullary cavity by H&E staining. The corresponding TRAP staining and immunohistochemical analysis also demonstrated the accumulation of osteoclasts and bacterial residues around the tibia medullary cavity for the Ti and Ti-PDA implants, suggesting the occurrence of bone resorption. In comparison, a large amount of woven bone was detected at the implant–tissue interface for the Ti-PDA-Zn sample as shown by Masson's trichrome staining. Moreover, no detectable signs of bacterium infection were observed for the Ti-PDA-Zn implant, suggesting that the Ti-PDA-Zn coating effectively eradicated bacteria and prevented implant-related infections.

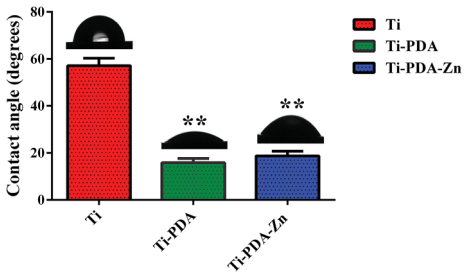

Fig. 5 Images of water drops on the surface of Ti, Ti-PDA, and Ti-PDA-Zn coatings. $^{**}p < 0.01$ *vs.* Ti.

Discussion

Orthopedic implants are widely used and highly successful treatments for musculoskeletal issues including trauma, osteoporotic diseases, bone cancer, and joint and spinal diseases. It has been estimated that by the end of 2030, the number of total

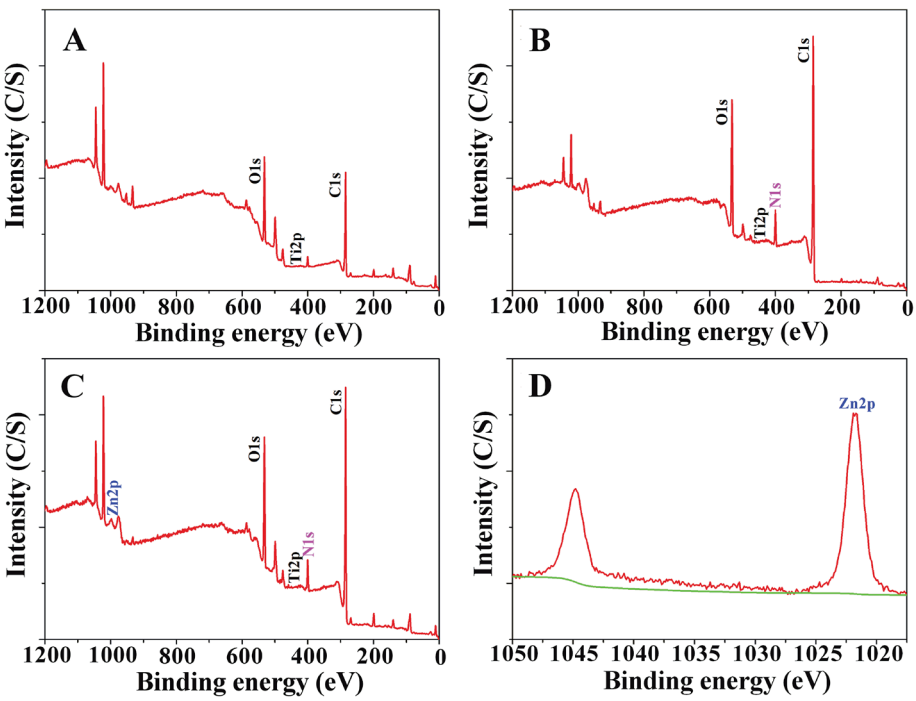

Fig. 4 XPS survey spectra of Ti (A); Ti-PDA (B); Ti-PDA-Zn (C); and high-resolution spectra of Zn 2p (D).

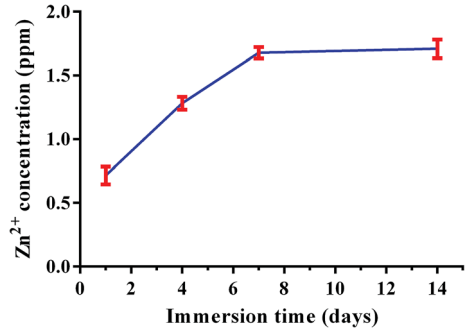

Fig. 6 Zn^{2+} concentrations in PBS solution after immersion for 1, 4, 7, and 14 days.

hip replacements and total knee arthroplasties will rise by 174% (572 000 procedures) and 673% (3.48 million procedures), respectively, in the United States.[33] However, the success of these treatments can be undermined by implant-related infections and insufficient osseointegration, the two leading causes of implant failure and complex revision surgeries.[34] For total joint arthroplasty, 20% of implant failures are attributed to infection.[35,36] In addition, recent studies point to the key role that microbes may play in initiating or accelerating implant failure pathways even in cases where infection is not the primary cause.[37] The annual cost for treating periprosthetic joint infection is projected to exceed $1.62 billion by 2020.[38] As demands for joint arthroplasty are expected to increase substantially over the coming decade, improvements in the overall function and lifetime of orthopedic implants are highly desirable not only to improve patients' well-being, but also to alleviate a huge economic burden on society. From the perspective of clinical applications, the ideal orthopedic implant coating to prevent or treat periprosthetic joint infections will likely be multifunctional to meet the various requirements. The implanted biomaterial must possess broad-spectrum antibacterial performance as a wide variety of bacteria can infect an implant, including Gram-positive and Gram-negative bacteria.[39] The implant also needs to exhibit excellent biological properties to promote osseointegration at the bone-implant interface, thereby limiting the chances of infection leading to osteolysis and implant loosening.[34,40]

In the present study, we have successfully fabricated Zn-surface-modified Ti substrates *via* PDA chemical surface modification to achieve both excellent biological and antibacterial performance. The successful formation of the PDA coating on the titanium substrate and anchoring of the Zn ions to the PDA coating through coordination interaction were confirmed by EDS and XPS (Fig. 3 and 4). It is known that Gram-positive *Staphylococcus* bacteria, most prominently *S. aureus* and *S. epidermidis* contribute to 70% of orthopedic implant infections, whereas Gram-negative bacteria, such as *E. coli* and *Klebsiella pneumoniae* cause approximately 5% of infections.[41–43] In addition, inhibition of invasive-bacteria spread as early as possible, especially within the first 6 h of the implantation surgery, helps to reduce the risk of biofilm formation, as the invading bacteria have not yet begun rapid proliferation.[44,45] We chose representative Gram-positive *S. aureus* and Gram-negative *E. coli* to evaluate the broad-spectrum antibacterial properties of the Ti-PDA-Zn coatings. The results showed that the Ti-PDA-Zn coating could effectively inhibit the growth of both *S. aureus* and *E. coli*, which may be attributed to the incorporation of Zn ions on the surface. Previous studies have confirmed that the antibacterial mechanism of zinc ion-decorated biomaterials can be mainly attributed to the destruction of cell membranes and the production of reactive oxygen species (ROS), eventually killing the bacterial cells.[16,46] Ning *et al.* have reported that the minimal inhibition concentration of Zn ions against both *S. aureus* and *E. coli* is 10^{-7} mol L^{-1}.[46] However, the highest concentration of Zn ions measured by ICP-AES in our study was ~1.7 ppm (Fig. 6). Therefore, the most likely antibacterial mechanism of the Ti-PDA-Zn coating is the generation of ROS. In addition, our studies demonstrate that *S. aureus* is more sensitive to the coating than *E. coli*, which may be attributed to differences in the cell membrane structures of the Gram-positive and Gram-negative bacteria.[12,47]

Assessing the biocompatibility of a coating is as important toward assessing the potential of the coating in biomedical applications. Zinc is an essential trace element that plays an important role in the structure and function of proteins and

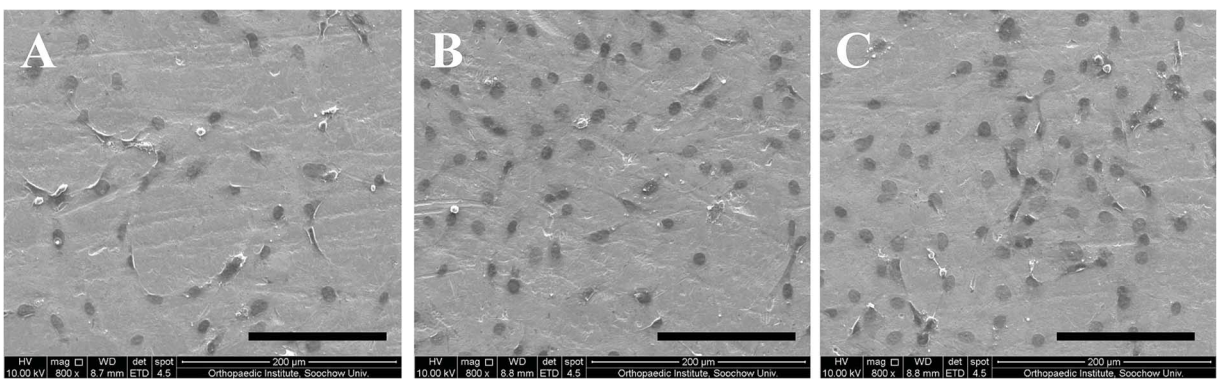

Fig. 7 Morphology of MC3T3-E1 cells cultured on Ti (A), Ti-PDA (B), and Ti-PDA-Zn (C) substrates for 24 h, as observed using SEM. Scale bars, 200 μm.

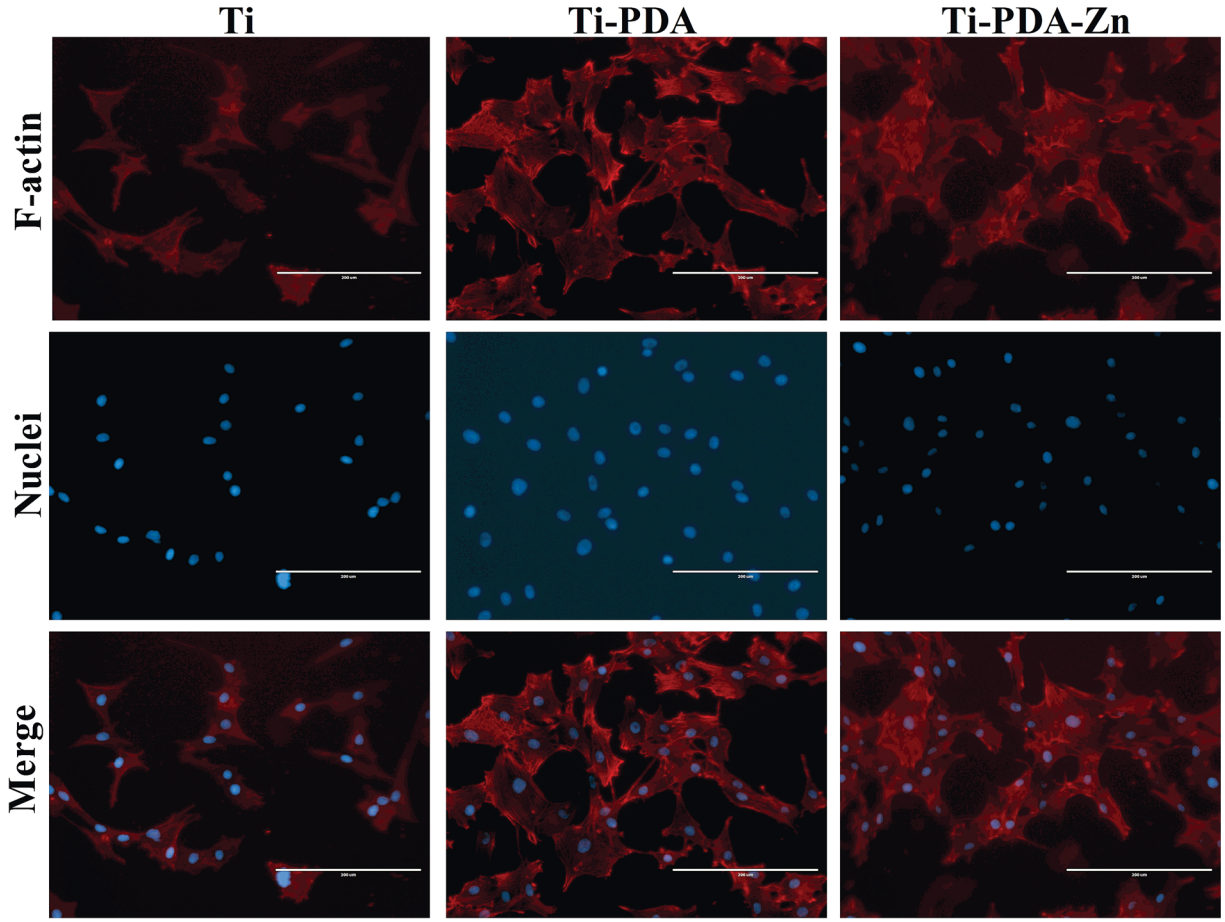

Fig. 8 Fluorescent images of MC3T3-E1 cells cultured on various surfaces for 24 h with actin stained with phalloidin (red) and nuclei stained with DAPI (blue). Scale bars, 200 μm.

a variety of cellular processes, including DNA synthesis, enzyme activity, and cell division.[48,49] In contrast, Zn ions in high concentrations would induce cellular toxicity.[49,50] In our study, the *in vitro* biocompatibility of the Ti-PDA-Zn coating was evaluated using MC3T3-E1 cells. It is well known that the initial adhesion of cells to the surface of an implant is a key step for subsequent cell proliferation and differentiation. The results of SEM and fluorescence microscopy showed that the amounts and skeletal structures of MC3T3-E1 cells on the different titanium substrates were significantly different (Fig. 7 and 8). The amount of MC3T3-E1 cells on the Ti-PDA and Ti-PDA-Zn surfaces was significantly higher than on the Ti surfaces. In addition, compared with the Ti substrate, the MC3T3-E1 cells incubated with the Ti-PDA and Ti-PDA-Zn coatings displayed better cell adhesion and spreading, as indicated by the higher cell density and irregular cell morphology with the development of numerous lamellipodia and filopodia processes. These results indicate that the PDA coating can promote initial cellular adhesion and spreading, which is consistent with the findings from previous studies.[28,29] According to the concept of the "race for the surface" as laid out by Gristina, if host cells first occupy the surface of the implant, this not only promotes tissue

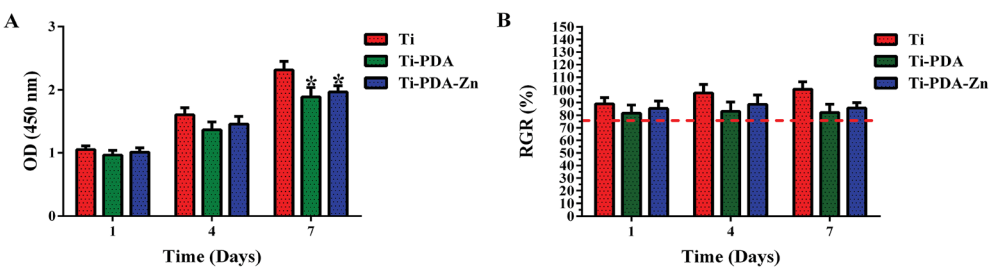

Fig. 9 (A) OD values in CCK-8 tests with Ti, Ti-PDA, and Ti-PDA-Zn coatings; (B) RGR values of cp-Ti, Ti-PDA, and Ti-PDA-Zn coatings with different incubation durations. *$p < 0.05$ *vs.* Ti.

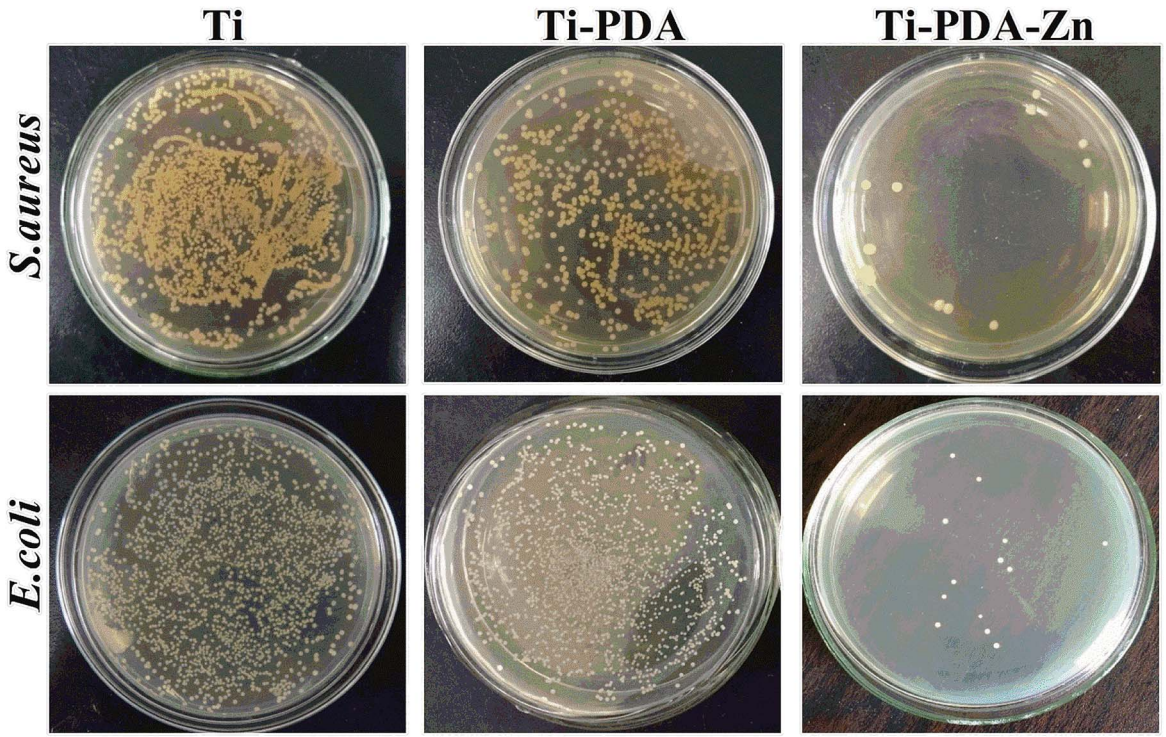

Fig. 10 Representative images of bacteria colonies on Ti, Ti-PDA, and Ti-PDA-Zn substrates after culturing for 24 h.

integration, but also helps build defensive barriers against the attachment and colonization of microbes.[51] To further investigate the cytotoxicity of the different Ti samples, the proliferative activity of MC3T3-E1 cells was determined by CCK-8 assay and the RGR was calculated. The results showed that the different Ti samples exerted no significant toxicity on the cells (Fig. 9). After culturing for 1 and 4 days, no differences could be found in the OD values of the Ti, Ti-PDA, and Ti-PDA-Zn samples. However, cell proliferation activity on the Ti-PDA and Ti-PDA-Zn samples was slightly lower than that on the Ti substrate ($p < 0.05$). In addition, the calculated RGR values at different culture times were all higher than 75%, implying that the cell biocompatibility of both the Ti-PDA and Ti-PDA-Zn coatings is as good as that of the Ti substrate. Previous studies have confirmed that Zn ion concentrations under 2 ppm are safe and would not lead to obvious cytotoxicity.[16] In our case, the release of Zn ions was measured by ICP-AES, and the highest concentration of Zn ions detected was 1.70 ± 0.07 ppm at 14 days, which is below the 2 ppm safe concentration. The above results thus provide

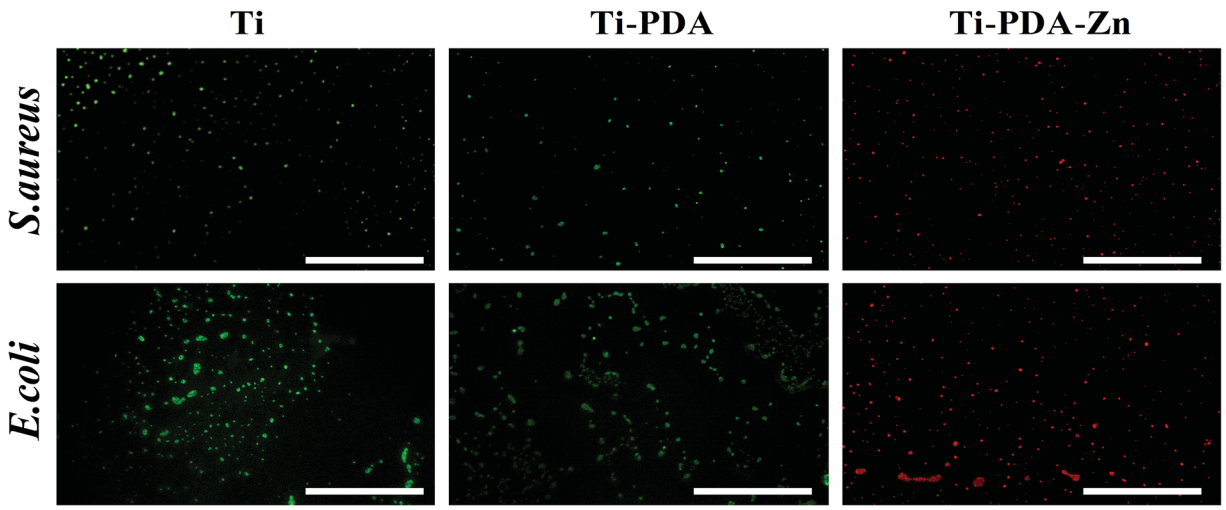

Fig. 11 Fluorescence staining photographs of bacteria cultured on tested samples; green fluorescence indicates live bacteria and red fluorescence indicates dead bacteria. Scale bars, 20 μm.

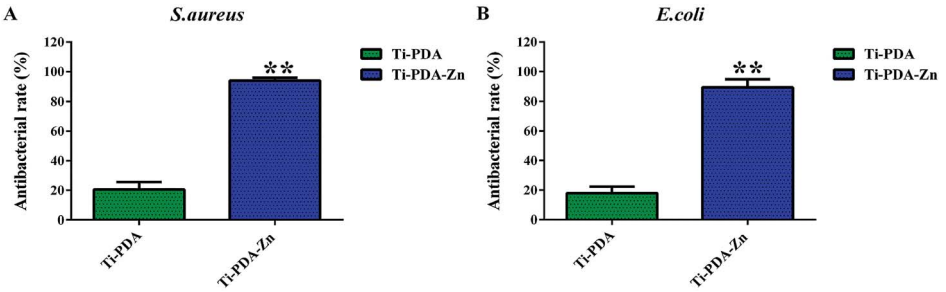

Fig. 12 Calculated antibacterial rates of Ti-PDA and Ti-PDA-Zn substrates against *S. aureus* (A) and *E. coli* (B) using the plate-counting method. $^{**}p < 0.01$ *vs.* Ti-PDA.

a strong basis for supporting the excellent antibacterial activities and good biocompatibility displayed by Ti-PDA-Zn coatings.

In 1975, Schurman *et al.* proposed the first model of joint infection in rabbits.[52] Since then, a variety animal models of periprosthetic joint infection have been successfully established, which not only help to better study the pathogenesis of implant-related infections, but also help to better evaluate the antibacterial properties and osseointegration effects of implanted biomaterials. These animal models can mimic both the micro-environment of the infection progress and bone growth.[53,54] Imaging and histology analyses are currently the main methods used to assess the osteogenic and anti-infection properties of biomaterials *in vivo*.[55] Contrary to the traditional X-ray examination, micro-CT analysis can quantitatively evaluate the infection-induced morphological changes of bone surrounding the implants *via* 3D reconstruction of the scanning

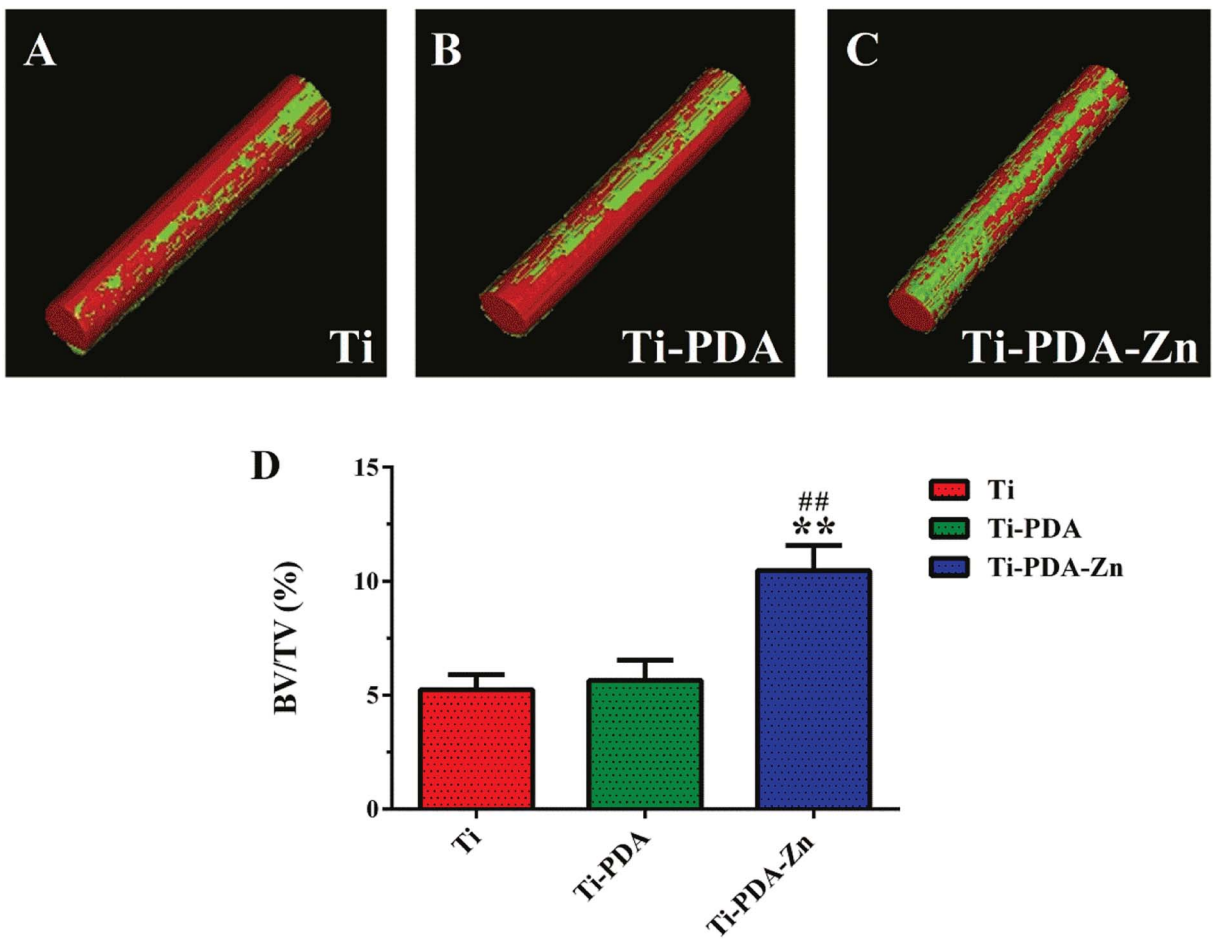

Fig. 13 Micro-CT 3D reconstructed models showing the status of osseointegration around Ti (A), Ti-PDA (B), and Ti-PDA-Zn (C) at 4 weeks after implantation (the red color represents the implant and the green color represents the bone tissue). (D) Bone volume fraction (BV/TV) of the three groups obtained from analysis of the Micro-CT data ($n = 4$). $^{**}p < 0.01$ *vs.* Ti and $^{\#\#}p < 0.01$ *vs.* Ti-PDA.

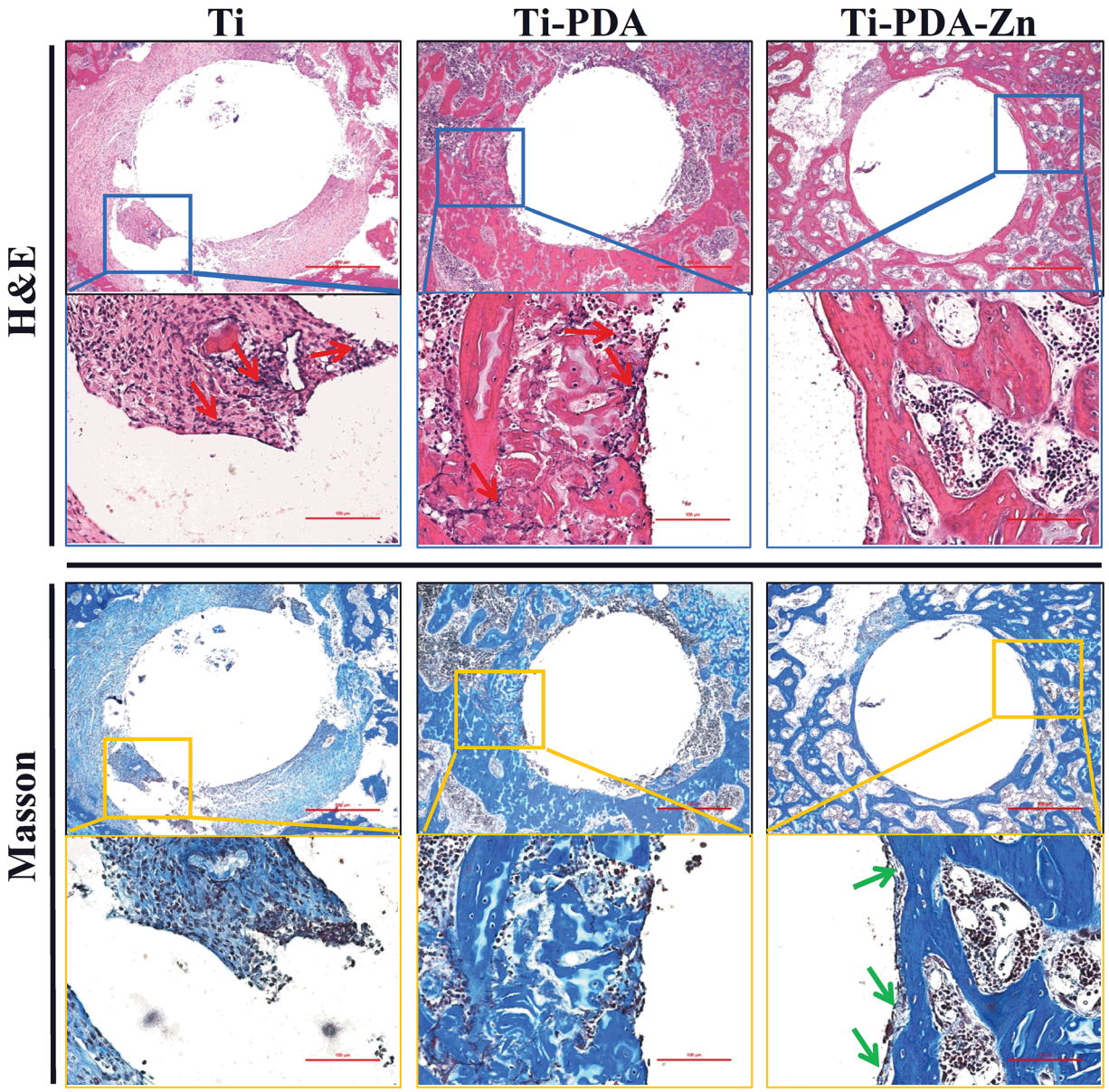

Fig. 14 High magnification histological images of H&E and Masson' trichrome staining at 4 weeks after surgery. Scale bars, 500 μm.

data and quantitative measurements of the ROI by imaging processing and analysis software.[55] There are few research studies related to assessing the osteogenic properties of Zn-decorated biomaterials in the presence of bacteria, although a number of experiments *in vitro* and *in vivo* have proved the osteogenic and anti-infection properties of zinc-related biomaterials separately.[12,16,48,56,57] An intramedullary implant approach was used herein to mimic periprosthetic infection, and the performance of the materials was systematically evaluated using micro-CT and histology analyses and immunohistochemistry. It is well known that stable connections in bone-implant interfaces are crucial to the clinical success of Ti implants. At the same threshold and VOI, CT scanning indicated that the Ti-PDA-Zn group had a higher percentage of BV/TV than the Ti and Ti-PDA samples, which agrees with the results of osteogenic differentiation of Zn-incorporated biomaterials.[14,15,57] Details at the bone–implant interface were then investigated by histological and immunohistochemistry staining. Four weeks after implantation, the bone tissues around the Ti and Ti-PDA implants were destroyed by implant-related osteomyelitis, as confirmed by the large number of neutrophils, and osteoclastic bone resorption, as well as bacterial residues around the tibia medullary cavity. In contrast, no sign of bacterial infection or bone resorption was detected around the Ti-PDA-Zn implant. Moreover, a large amount of woven bone was observed at the implant–tissue interface for the Ti-PDA-Zn implant as shown by Masson's trichrome staining, which was consistent with the micro-CT results. It is believed that *S. aureus* exerts an effect on both osteoblasts and osteoclasts. Osteoblast infection by *S. aureus* can lead to reduced

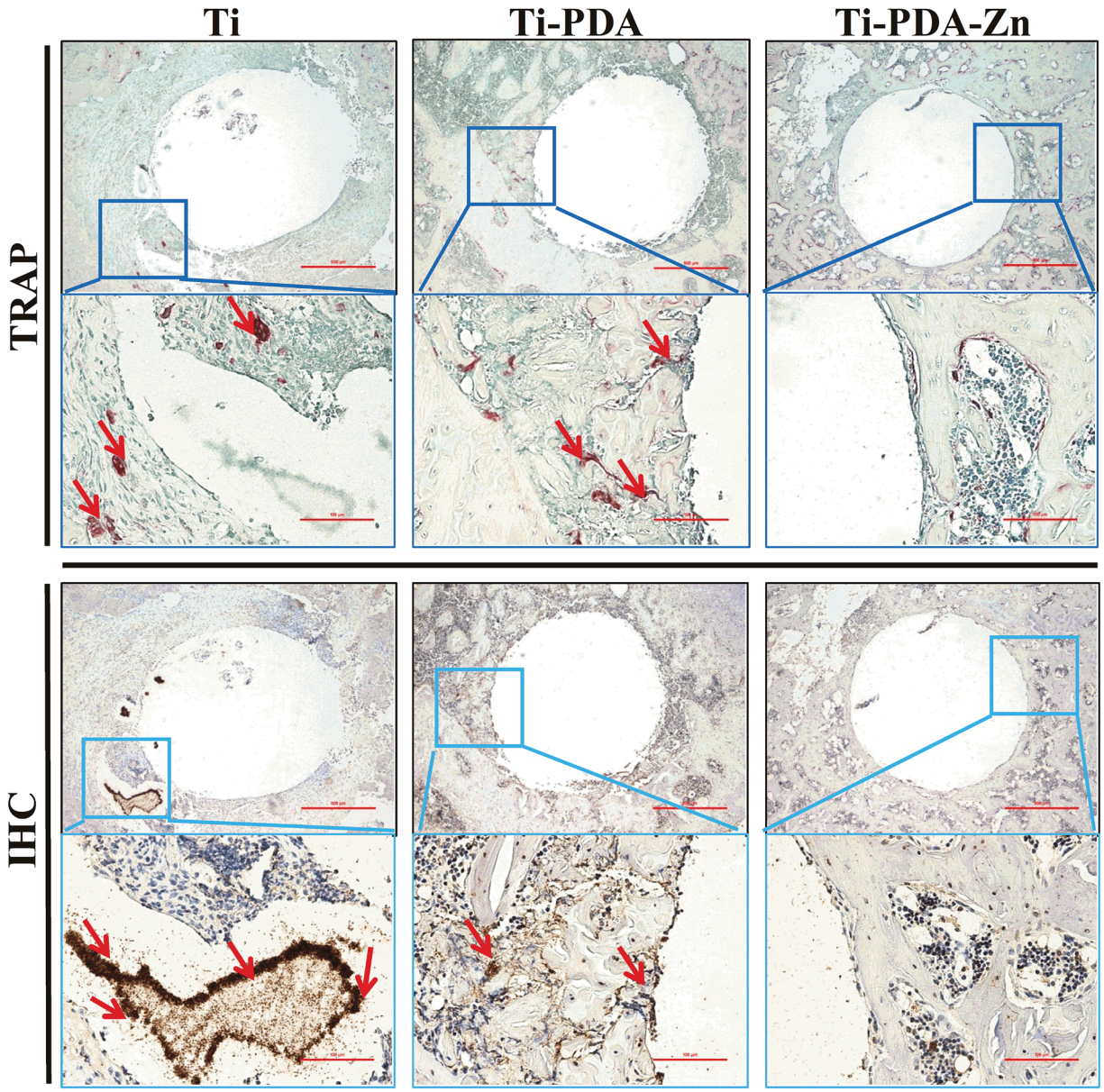

Fig. 15 High magnification histological images of TRAP and immunohistochemical staining at 4 weeks after surgery. Scale bars, 500 μm.

bone formation activity and osteoblast death.[58] Osteoclasts infected by *S. aureus* can enhance bone resorption activity, and the aggregation of osteoclasts in the infected areas is mediated by the pro-inflammatory and pro-osteoclastogenic factors resulting from immune responses,[31] which is consistent with the results of histological sections and immunohistochemistry staining in our research. Taken together, the results from the animal model of implant-related infections demonstrated that the Ti-PDA-Zn coating possesses both excellent antibacterial properties and improved osseointegration capability in the presence of *S. aureus in vivo*. These properties are mainly attributable to the antibacterial effects of the zinc ions, which reduce the activity of the osteoclasts mediated by *S. aureus* and reduce infected bone destruction.

The results from the *in vitro* and *in vivo* studies demonstrated that the Ti-PDA-Zn coating exhibits excellent antibacterial activity, good biocompatibility, as well as enhanced osseointegration performance. Thus, it is expected that Ti-PDA-Zn can help prevent surgical site infections associated with total joint replacement in the early postoperative period.

Conclusion

We have developed a bi-functional film in which zinc ions are immobilized on a Ti substrate *via* PDA chemical surface modification. The resulting Ti-PDA-Zn coating demonstrated excellent antibacterial activities and good biocompatibility *in vitro*. The results from the animal model of implant-related infections demonstrated that the Ti-PDA-Zn coating displayed both excellent antibacterial properties and enhanced osseointegration capability in the presence of *S. aureus in vivo*. In addition, the preparation of the coating has many advantages,

including ease-of-use, versatility, and high stability under physiological conditions. Together, the findings from this study indicate that the Ti-PDA-Zn coating is a promising candidate for orthopedic implants, exhibiting both antimicrobial and regenerative properties.

Author contributions

Conceptualization, Lei Wang, Xifu Shang, and Yuefeng Hao; methodology, Guoyang Wan, Lei Wang, Xifu Shang, and Yuefeng Hao; validation, Lijun Dong and Degang Huang; formal analysis, Junying Sun, and Xing Yang; data curation, Xin Yang; writing—original draft preparation, Lei Wang, Xifu Shang and Yuefeng Hao; writing—review and editing, Qiang Wang, Guochun Zha, and Xing Yang; project administration, Qiang Wang, Guochun Zha, and Xing Yang.

Conflicts of interest

There are no conflicts to declare.

Acknowledgements

This work was supported by the Special Scientific Research Fund for Introducing Talents in Yijishan Hospital, National Natural Science Foundation of China (Grant no. 81472060), Program for Construction of Suzhou Clinical Medical Center of Orthopaedics and Burns (Grant no. szzxj201506), Program for Introduction of Clinical Medical Teams to Suzhou (Grant no. szyjtd201714), Program from Jiangsu Health and Health Committee (Grant no. H2018027) and Social Development Program from Suzhou Science and Technology Bureau (Grant no. sys201427, sysd2015118, sysd2017170, sysd2018207).

References

1 Y. Kirmanidou, M. Sidira, M. E. Drosou, V. Bennani, A. Bakopoulou, A. Tsouknidas, N. Michailidis and K. Michalakis, *BioMed Res. Int.*, 2016, **2016**, 2908570.
2 W. J. Metsemakers, K. Kortram, M. Morgenstern, T. F. Moriarty, I. Meex, R. Kuehl, S. Nijs, R. G. Richards, M. Raschke, O. Borens, S. L. Kates, C. Zalavras, P. V. Giannoudis and M. H. J. Verhofstad, *Injury*, 2018, **49**, 497–504.
3 R. A. Henderson and M. S. Austin, *J. Arthroplasty*, 2017, **32**, 2056–2059.
4 E. M. Hetrick and M. H. Schoenfisch, *Chem. Soc. Rev.*, 2006, **35**, 780–789.
5 S. Ferraris and S. Spriano, *Mater. Sci. Eng., C*, 2016, **61**, 965–978.
6 R. Kargupta, S. Bok, C. M. Darr, B. D. Crist, K. Gangopadhyay, S. Gangopadhyay and S. Sengupta, *Wiley Interdiscip. Rev.: Nanomed. Nanobiotechnol.*, 2014, **6**, 475–495.
7 J. A. Inzana, E. M. Schwarz, S. L. Kates and H. A. Awad, *Biomaterials*, 2016, **81**, 58–71.
8 D. P. Lew and F. A. Waldvogel, *Lancet*, 2004, **364**, 369–379.
9 A. J. Tande, E. O. Gomez-Urena, E. F. Berbari and D. R. Osmon, *Infect. Dis. Clin. North Am.*, 2017, **31**, 237–252.
10 R. O. Darouiche, *N. Engl. J. Med.*, 2004, **350**, 1422–1429.
11 T. N. Phan, T. Buckner, J. Sheng, J. D. Baldeck and R. E. Marquis, *Oral Microbiol. Immunol.*, 2004, **19**, 31–38.
12 H. Hu, W. Zhang, Y. Qiao, X. Jiang, X. Liu and C. Ding, *Acta Biomater.*, 2012, **8**, 904–915.
13 J. X. Wang, H. J. Zhou, G. Y. Guo, J. Q. Tan, Q. J. Wang, J. Tang, W. Liu, H. Shen, J. H. Li and X. L. Zhang, *ACS Appl. Mater. Interfaces*, 2017, **9**, 33609–33623.
14 Y. Q. Liang, J. Xu, J. Chen, M. C. Qi, X. H. Xie and M. Hu, *Mol. Med. Rep.*, 2015, **11**, 4225–4231.
15 K. Yusa, O. Yamamoto, H. Takano, M. Fukuda and M. Iino, *Sci. Rep.*, 2016, **6**, 29462.
16 X. K. Shen, Y. Hu, G. Q. Xu, W. Z. Chen, K. Xu, Q. C. Ran, P. P. Ma, Y. R. Zhang, J. H. Li and K. Y. Cai, *ACS Appl. Mater. Interfaces*, 2014, **6**, 16426–16440.
17 K. Li, J. M. Yu, Y. T. Xie, L. P. Huang, X. J. Ye and X. B. Zheng, *J. Mater. Sci.: Mater. Med.*, 2011, **22**, 2781–2789.
18 Y. H. Chen, G. W. Wu and J. L. He, *Mater. Sci. Eng., C*, 2015, **48**, 41–47.
19 Y. Yu, G. Jin, Y. Xue, D. Wang, X. Liu and J. Sun, *Acta Biomater.*, 2017, **49**, 590–603.
20 J. He, W. Feng, B. H. Zhao, W. Zhang and Z. Lin, *Int. J. Oral Maxillofac. Implants*, 2018, **33**, 298–310.
21 J. Bejarano, P. Caviedes and H. Palza, *Biomed. Mater.*, 2015, **10**, 025001.
22 M. Li, X. M. Liu, Z. Q. Xu, K. W. K. Yeung and S. L. Wu, *ACS Appl. Mater. Interfaces*, 2016, **8**, 33972–33981.
23 N. Khoshnood, A. Zamanian and A. Massoudi, *Mater. Sci. Eng., C*, 2017, **77**, 748–754.
24 H. Lee, J. Rho and P. B. Messersmith, *Adv. Mater.*, 2009, **21**, 431–434.
25 C. C. Gao, Y. Wang, F. X. Han, Z. Q. Yuan, Q. Li, C. Shi, W. W. Cao, P. H. Zhou, X. D. Xing and B. Li, *J. Mater. Chem. B*, 2017, **5**, 9326–9336.
26 L. Wang, X. Yang, W. W. Cao, C. Shi, P. H. Zhou, Q. Li, F. X. Han, J. Y. Sun, X. D. Xing and B. Li, *RSC Adv.*, 2017, **7**, 51593–51604.
27 J. H. Kim, M. K. Joshi, J. Lee, C. H. Park and C. S. Kim, *J. Colloid Interface Sci.*, 2018, **513**, 566–574.
28 S. H. Ku, J. Ryu, S. K. Hong, H. Lee and C. B. Park, *Biomaterials*, 2010, **31**, 2535–2541.
29 W. B. Tsai, W. T. Chen, H. W. Chien, W. H. Kuo and M. J. Wang, *Acta Biomater.*, 2011, **7**, 4187–4194.
30 S. Zhong, R. Luo, X. Wang, L. Tang, J. Wu, J. Wang, R. Huang, H. Sun and N. Huang, *Colloids Surf., B*, 2014, **116**, 553–560.
31 S. Trouillet-Assant, M. Gallet, P. Nauroy, J. P. Rasigade, S. Flammier, P. Parroche, J. Marvel, T. Ferry, F. Vandenesch, P. Jurdic and F. Laurent, *J. Infect. Dis.*, 2015, **211**, 571–581.
32 H. Cheng, Y. Li, K. Huo, B. Gao and W. Xiong, *J. Biomed. Mater. Res., Part A*, 2014, **102**, 3488–3499.
33 S. M. Kurtz, K. L. Ong, J. Schmier, F. Mowat, K. Saleh, E. Dybvik, J. Karrholm, G. Garellick, L. I. Havelin, O. Furnes, H. Malchau and E. Lau, *J. Bone Jt. Surg., Am. Vol.*, 2007, **89a**, 144–151.

34 J. Raphel, M. Holodniy, S. B. Goodman and S. C. Heilshorn, *Biomaterials*, 2016, **84**, 301–314.
35 K. J. Bozic, S. M. Kurtz, E. Lau, K. Ong, V. Chiu, T. P. Vail, H. E. Rubash and D. J. Berry, *Clin. Orthop. Relat. Res.*, 2010, **468**, 45–51.
36 K. J. Bozic, S. M. Kurtz, E. Lau, K. Ong, T. P. Vail and D. J. Berry, *J. Bone Jt. Surg., Am. Vol.*, 2009, **91**, 128–133.
37 E. M. Greenfield, Y. M. Bi, A. A. Ragab, V. M. Goldberg, J. L. Nalepka and J. M. Seabold, *J. Biomed. Mater. Res., Part B*, 2005, **72b**, 179–185.
38 S. M. Kurtz, E. Lau, H. Watson, J. K. Schmier and J. Parvizi, *J. Arthroplasty*, 2012, **27**, 61–65 e61.
39 R. J. Holleyman, P. Baker, A. Charlett, K. Gould and D. J. Deehan, *Knee Surg. Sports Traumatol. Arthrosc.*, 2016, **24**, 3080–3087.
40 J. Pajarinen, E. Jamsen, Y. T. Konttinen and S. B. Goodman, *J. Long Term Eff. Med. Implants*, 2014, **24**, 283–296.
41 L. Pulido, E. Ghanem, A. Joshi, J. J. Purtill and J. Parvizi, *Clin. Orthop. Relat. Res.*, 2008, **466**, 1710–1715.
42 W. Zimmerli, A. Trampuz and P. E. Ochsner, *N. Engl. J. Med.*, 2004, **351**, 1645–1654.
43 B. H. Kapadia, R. A. Berg, J. A. Daley, J. Fritz, A. Bhave and M. A. Mont, *Lancet*, 2016, **387**, 386–394.
44 M. Emmerson, *New Horiz.*, 1998, **6**, S3–S10.
45 K. G. Neoh, X. F. Hu, D. Zheng and E. T. Kang, *Biomaterials*, 2012, **33**, 2813–2822.
46 C. Ning, X. Wang, L. Li, Y. Zhu, M. Li, P. Yu, L. Zhou, Z. Zhou, J. Chen, G. Tan, Y. Zhang, Y. Wang and C. Mao, *Chem. Res. Toxicol.*, 2015, **28**, 1815–1822.
47 K. M. Reddy, K. Feris, J. Bell, D. G. Wingett, C. Hanley and A. Punnoose, *Appl. Phys. Lett.*, 2007, **90**, 2139021–2139023.
48 G. Jin, H. Cao, Y. Qiao, F. Meng, H. Zhu and X. Liu, *Colloids Surf., B*, 2014, **117**, 158–165.
49 P. Liu, Y. Zhao, Z. Yuan, H. Ding, Y. Hu, W. Yang and K. Cai, *Mater. Sci. Eng., C*, 2017, **75**, 998–1005.
50 W. Watjen, H. Haase, M. Biagioli and D. Beyersmann, *Environ. Health Perspect.*, 2002, **110**(suppl. 5), 865–867.
51 A. G. Gristina, *Science*, 1987, **237**, 1588–1595.
52 D. J. Schurman, B. L. Johnson Jr and H. C. Amstutz, *J. Bone Jt. Surg., Am. Vol.*, 1975, **57**, 40–49.
53 A. B. Lovati, M. Bottagisio, E. de Vecchi, E. Gallazzi and L. Drago, *Adv. Exp. Med. Biol.*, 2017, **971**, 29–50.
54 L. Gatin, A. Saleh-Mghir, P. Massin and A. C. Cremieux, *Orthop. Traumatol. Surg. Res.*, 2015, **101**, 851–855.
55 X. Lin, S. Yang, K. Lai, H. Yang, T. J. Webster and L. Yang, *Nanomedicine*, 2017, **13**, 123–142.
56 K. Huo, X. Zhang, H. Wang, L. Zhao, X. Liu and P. K. Chu, *Biomaterials*, 2013, **34**, 3467–3478.
57 Y. Qiao, W. Zhang, P. Tian, F. Meng, H. Zhu, X. Jiang, X. Liu and P. K. Chu, *Biomaterials*, 2014, **35**, 6882–6897.
58 J. Josse, F. Velard and S. C. Gangloff, *Front. Cell. Infect. Microbiol.*, 2015, **5**, 85.